First principles study of hydrogen storage material $NaBH_4$ and $LiAlH_4$ compounds: electronic structure and optical properties

2016 Phys. Scr. 91 045804

(http://iopscience.iop.org/1402-4896/91/4/045804)

IOP Publishing | Royal Swedish Academy of Sciences Physica Scripta

Phys. Scr. **91** (2016) 045804 (18pp) doi:10.1088/0031-8949/91/4/045804

First principles study of hydrogen storage material $NaBH_4$ and $LiAlH_4$ compounds: electronic structure and optical properties

T Ghellab[1,2], Z Charifi[1], H Baaziz[1], Ş Uğur[3], G Uğur[3] and F Soyalp[4]

[1] Department of Physics, Faculty of Science, University of M'sila, 28000 M'sila, Algeria
[2] Department of Physics, Faculty of Science, University of Batna, 05000 Batna, Algeria
[3] Department of Physics, Faculty of Science, Gazi University 06500 Ankara, Turkey
[4] Yüzüncü Yıl University, Faculty of Education, Department of Physics, Van 65080, Turkey

E-mail: charifizoulikha@gmail.com

Received 24 June 2015, revised 14 February 2016
Accepted for publication 25 February 2016
Published 17 March 2016

Abstract

A comprehensive study of structure, phase stability, optical and electronic properties of $LiAlH_4$ and $NaBH_4$ light-metal hydrides is presented. The calculations are carried out within density functional theory using the full potential linear augmented plane wave method. The exchange-correlation potential is treated within the local density approximation and the generalized gradient approximation (GGA) to calculate the total energy. Furthermore, the Engel–Vosko GGA approach is employed to compute electronic and optical properties such as reflectivity spectra. The phases α, β and γ of $LiAlH_4$ and $NaBH_4$ hydrides are investigated, the phase transition from the β to the high-pressure γ phase is determined for $NaBH_4$ and is accompanied by a 1% volume decrease. For $LiAlH_4$, no phase transition is detected. The materials under consideration are classified as wide band gap compounds. From the analysis of the structures at different phases, it is deduced that the hydrides show strong covalent interaction between B (Al) and H in the $[BH_4]^-$ ($[AlH_4]^-$) anions and ionic bonding character between $[BH_4]^-$ and Na^+ for $NaBH_4$, and $[AlH_4]^-$ and Li^+ for $LiAlH_4$. The complex dielectric function, absorption coefficient and the reflectivity spectra are also computed and analyzed in different phases.

Keywords: hydrogen storage materials, high pressure, DFT, stability, structure, hydrides, phase transition

(Some figures may appear in colour only in the online journal)

1. Introduction

Hydrogen energy is one of the alternative energy candidates that could replace fossil fuels. It has received worldwide attention, and increased research interest, due to its sustainable, clean, and environmentally friendly properties. Several different methods of storing hydrogen are available. Hydrogen can be stored in gaseous form at high pressures in composite cylinders; it can also be stored as a liquid in a cryogenic tank at around 20° K at ambient pressure; or it can be stored in solid state materials [1, 2]. This final alternative is being considered as the most efficient and feasible approach to using hydrogen.

Discovering new hydrogen storage materials which fulfill all the requirements relating to high reversibility, hydrogen capacity, moderate reaction temperature and pressure at ambient conditions, good absorption and desorption kinetics [3], and efficiency at the required operating temperature range are necessary to implement fuel cell technology for transportation applications. In the last few years, there has been considerable research and development in the use of novel condensed-phase hydride materials for hydrogen storage [4–6]. Solid metal hydrides offer the largest volumetric density and they are now considered to be the most safe and effective way to store hydrogen. The reason why hydrogen storage materials are so important to be investigated is that there are

so many different lightweight compounds that store hydrogen, some of which have reversible properties at reasonable temperatures below 250 °C. Recently, there has been a notably rapid evolution of this domain, and a lot of studies on the determination of structures of crystals, bonding properties and phase transitions have been carried out of complex hydrides [4, 7–12] at different pressure–temperature conditions.

In order to find effective hydrogen storage materials with breakthrough performance complex hydrides such as borohydrides [4, 7–11, 13] and alanates [5, 12] have received much attention due to their extremely volumetric hydrogen densities and high gravimetric factor. A large volume collapse for high-pressure phases of $LiAlH_4$ and $NaAlH_4$ was predicted [5, 12]. Talyzin *et al* performed a set of experiments using the diamond anvil cell. They observed a phase transition from α-$LiBH_4$ to β-$LiBH_4$ high-pressure phase using x-ray diffraction and Raman spectroscopy between 0.8 and 1.1 GPa [4].

On the basis of first principles studies, it was indicated that at low temperature the most stable phase is the orthorhombic while the hexagonal ($P6_3mc$) structure experimentally proposed is the most stable phase at high temperature. Furthermore, a new phase at high temperature was discovered which is the monoclinic ($C2/c$) one [11]. The electronic structure and the phase stability of $LiAlH_4$ using density functional theory (DFT) calculations have been studied [5]. Seven close structure types have been considered; a phase transition from α-$LiAlH_4$ to β-$LiAlH_4$ has been found at arround 3 GPa accompanied by a huge volume decrease. At high pressure the β phase transforms to γ-$LiAlH_4$ with a negligible volume collapse and an increased coordination number of Al from four to six. The high-pressure β phases of $LiAlH_4$ and $NaAlH_4$ compounds keep in reserve hydrogen more volume efficient than the corresponding α phases. The determinination of the kinetic and thermodynamic parameters, and the temperature at which induced decomposition mechanisms of the intermediate phases for hydrogen storage in $LiAlH_4$ occur have been reported [14]. In addition, this hydride was predicted to be an insulator with a band gap of 4.6 eV.

Basic research in hydrogen storage needs to focus on understanding the structural, thermodynamic, physical, and bonding properties of light-metal hydrides such as $NaAlH_4$, $LiAlH_4$, $NaBH_4$, and $LiBH_4$. $LiBH_4$ has four different phases: two at high pressure and two at ambient pressure. The low-temperature phase has Pnma symmetry [10, 15, 16]. It transforms into a hexagonal wurtzite-like ($P6_3mc$ space group symmetry) high-temperature phase at around 380° K [17, 18]. At a pressure range of 1.2–10 GPa and ambient temperature, $LiBH_4$ crystallizes in a new phase with Ama2 structure [19]. It can be considered as an orthorhombically distorted antistructure of PtS. Above 10 GPa another $LiBH_4$ phase forms [19]. It is isostructural to the cubic $NaBH_4$ (Fm-3m structures). It has been proposed experimentally that the orthorhombic Pnma phase is energetically the most favorable phase at low temperature whereas the hexagonal $P6_3mc$ phase is the most favorable high-temperature phase. In addition, a new monoclinic phase with space group $C2/c$ was discovered, which is competitive in stability with the $P6_3mc$ phase at high temperature [11]. This latter phase was predicted to be vibrationally unstable by DFT simulations [20] and instead a primitive cell having space group $P2_1/c$ is found to be the ground state phase at high temperature [21].

The calculated transition entalpy in $NaBH_4$ is consistent with a transformation from the fully disordered cubic phase (Fm-3m) at high temperature [22] to an ordered tetragonal phase at low temperature. Filinchuk *et al* observed phase transitions in $NaBH_4$ near 6 and 8 GPa in to the tetragonal ($P\bar{4}2_1c$) and orthorombic (Pnma) phases, respectively [23]. Vajeeston *et al* found that $NaBH_4$ crystallizes in the tetragonal $P4_2/nmc$ structure at low temperature, and they obtained the $P4_2/nmc$ phase lower in energy than the $P\bar{4}2_1c$ and Fm-3m by about 6 and 27 MeV, respectively [10]. Kim *et al* [24] considered Fm-3m, $P\bar{4}2_1c$ and Pnma phases of $NaBH_4$ in Car–Parrinello molecular dynamics calculations. They obtained that the tetragonal $P\bar{4}2_1c$ phase at zero temperature and pressure is more favorable than that of $P4_2/nmc$ symmetry. Crystal structure prediction of $NaBH_4$ from DFT calculations has been carried out [25], and the tetragonal ground state phase ($P4_2/nmc$) has been found to have the lowest energy, the monoclinic stable structure was recognized to be 22.75 kJ mol^{-1} above the ground state one at $T = 298°$ K, and two other structure, cubic and orthorhombic phases were recovered with Pnma and $F\bar{4}3m$ symmetries. The pressure–temperature phase diagram of $NaBH_4$ computed with a first principles method [26], and experimentally using combined raman spectroscopy and synchrotron x-ray diffraction [27], has been reported and the estimated temperature of the transition from cubic to tetragonal phase at 0 GPa is found to be 133° K [26].

$LiAlH_4$ crystallizes in the monoclinic α-phase (space group $P2_1/c$). Four hydrogen atoms surrounded Al in an almost regular tetrahedral configuration [14]. At ambient conditions $NaAlH_4$ crystallizes in the tetragonal phase with space group $I4_1/a$ [28]. The stability of XYH_4 and X_3YH_6 (X = Na, Li, K; Y = Al, Ga, B) compounds in the Na_3AlH_6 and $NaAlH_4$ structural types have been investigated. Replacement of an Al atom by a Ga or B atom decreases significantly the stability of the intermediate Na_3AlH_6 material [29]. The total energies of $NaAlH_4$ have been calculated using the projected augmented plane. At higher pressure, at about 6.43 GPa, α-$NaAlH_4$ transforms to an orthorhombic $SrMgH_4$-type structure (space group Cmc21 β-$NaAlH_4$) with a volume reduction of 4% [5]. First principles investigation of the electronic structure, the band gaps and the optical properties of metal hydrides, the simple hydrides MgH_2, NaH, LiH, and AlH_3, and the complex hydrides Na_3AlH_6, Li_3AlH_6, $NaAlH_4$, $LiAlH_4$, and $Mg(AlH_4)_2$ has been reported [30]. Na_3AlH_6, AlH_3, and LiH have a direct band gap, whereas in all the other compounds the band gap is indirect. The thermodynamic properties, the dehydriding temperature and pressure of $Na_{1-x}Z_xAl_{1-y}D_yH_4$ (Z = Li, K, D = B, Ga) complex hydrides have been discussed and reported [31]. $Na_{1-x}Li_xAl_{1-y}B_yH_4$ complex hydrides are expected to deliver a huge quantity of hydrogen in a smaller range of pressure and temperature.

The main focus of this work is hydrogen storage in alkali metal based hydrides, in particular the hydrogen storage properties of complex hydrides based on Li and Na. The main motivation for studying complex hydrides is obviously their potential in storing large amounts of hydrogen at relatively low temperature (~100 °C). Computer simulation can be a powerful tool in characterizing the structures of $NaBH_4$ and $LiAlH_4$ compounds, and in understanding various properties such as electronic and optical ones. In section 2 we report the computational methods used in our study. The results discussed in this paper are obtained using DFT and are presented in sections 3.1, 3.2 and 3.3 respectively. In section 3.1, we describe the different structures of $NaBH_4$ and $LiAlH_4$ compounds and their stabilities. We focus on the electronic properties in terms of band structures, density of states (DOS) in section 3.2. In section 3.3 the optical properties are presented and discussed and finally, section 4 summarizes our results.

2. Computational details and crystal structures of materials

The complex hydrides X_a $(YH_m)_b$ formed of a group of compounds, where X is an alkaline earth or alkali element, Y is B, N or Al, and m is 1, 2, 4 or 6, the number of hydrogen atoms surrounding some other atom (such as Al, B, or N). The so-called complex hydrides are ionic compounds of $[AlH_4]^-$ or $[BH_4]^-$ anions and cations, usually from the alkali or the alkaline earth metals such as $NaAlH_4$ and $LiBH_4$.

Co-existence of both covalent and ionic types of bonding adds flexibility in adjusting their thermal stability. In ternary hydrides of main group metals such as $NaAlH_4$, hydrogen covalently bonds with Al to form tetrahedral anions $[AlH_4]^-$, which then interact ionically with Na^+ cations [32]. The position of hydrogen (H) atoms is hard to identify using x-ray diffraction because H has just one electron comparing to other elements in the periodic table [33]. Therefore we determine atomic positions and total energies for the considered structures of $NaBH_4$ and $LiAlH_4$ hydrides through full geometry optimization.

Ab initio calculations for different phases of $NaBH_4$ and $LiAlH_4$ hydrides were carried out using the full potential linearized augmented plane wave (FP-LAPW) method. We use the WIEN2K [34] implementation of the method that allows the inclusion of local orbitals in the basis, improving upon linearization and making possible a consistent treatment of the semicore and valence states in an energy window, hence ensuring proper orthogonality. The exchange-correlation potential is treated within local density approximation (LDA) and generalized gradient approximation (GGA) by Perdew, parametrized by Burke and Ernzerhof (PBE) [35]. Furthermore, for the electronic and optical properties we also used the Engel–Vosko (EV-GGA) approach [36]. The spherical harmonic expansion is used inside the muffin-tin sphere, and the plane wave basis set is chosen outside the sphere. Inside the atomic spheres the charge density and the potential are expanded in spherical harmonics up to $l_{max} = 10$. The density–plane wave cut-off is $RK_{max} = 9$, while the potential cut-off extends up to 12, so no shape approximation to the potential is necessary. R_{MT} is taken to be 0.8–1.6 atomic units (a.u.) for Na, Li, B, Al, and H atoms for all phases. Brillouin zone (BZ) integrations within the self-consistency cycles were performed via a tetrahedron method [37, 38], using 35 $\boldsymbol{k}$ points for α phase and 60 $\boldsymbol{k}$ points in the irreducible BZ (IBZ) for both β and γ phases for $NaBH_4$; for $LiAlH_4$, 99 $\boldsymbol{k}$ points, 105 $\boldsymbol{k}$ points and 80 $\boldsymbol{k}$ points in the IBZ for α phase, β phase and γ phase in the IBZ, respectively. For the calculation of the electronic, the DOS and the optical properties, however, a denser sampling of uniformly distributed $\boldsymbol{k}$ points is required, Hence, the Brillouin zone integration was performed, for $NaBH_4$ using 560 $\boldsymbol{k}$ points in the IBZ for the cubic phase and 1320 $\boldsymbol{k}$ points for the tetragonal phase of both β and γ phases, and for the $LiAlH_4$ compound, 2430 $\boldsymbol{k}$ points in the IBZ for the monoclinic phase, 2562 $\boldsymbol{k}$ points in the IBZ for the tetragonal phase, and 2704 $\boldsymbol{k}$ points in the IBZ for the orthorhombic phase are used. When the energy difference was less than 0.1 mRy, convergence was assumed.

To completely determine the stability of a specific phase, the Gibbs energy has to be established and its minima should be calculated. It is given by [39]:

$$G = E_{tot} + PV - TS. \tag{1}$$

The theoretical calculations are done at 0 K, so the free energy becomes equal to the enthalpy (H):

$$H = E_{tot} + PV. \tag{2}$$

At a given pressure, the stable phase is that with the lowest enthalpy and the transition pressure is calculated at which the enthalpies for the two phases are equal.

The calculation of the dielectric functions involve the energy eigenvalues and electron wave functions. The interband contribution to the imaginary part $\varepsilon_2(\omega)$ of the dielectric function is given by [40] for cubic phase:

$$\varepsilon_2(\omega) = \frac{8}{3\pi\omega^2}\sum_{nn'}\int_{BZ} |P_{nn'}(\boldsymbol{k})|^2 \frac{dS_{\boldsymbol{k}}}{|\nabla_{\boldsymbol{k}}\omega_{nn'}(\boldsymbol{k})|}. \tag{3}$$

The above expression is written in Rydberg atomic units with $e^2 = 1/m = 2$ and $\hbar = 1$.

Here $\omega_{nn'}(k)$ is the photon energy (Ry).

Where $P_{nn'}(k)$ is the dipolar matrix elements between the initial $|nk\rangle$ and final $|n'k\rangle$ states with their eigenvalues $E_n(k)$ and $E_{n'}(k)$, respectively. $\omega_{nn'}(k)$ is the energy difference,

$$\omega_{nn'}(k) = E_n(k) - E_{n'}(k)$$

and S_k is a constant energy surface

$$S_k = \{k;\ \omega_{nn'}(k) = \omega\}.$$

The real part $\varepsilon_1(\omega)$ can be estimated from $\varepsilon_2(\omega)$ using the Kramers–Kronig expressions and is given by [41].

The reflectivity $R(\omega)$, the absorption coefficient $I(\omega)$, refractive index $n(\omega)$, and extinction coefficient $k(\omega)$ in the

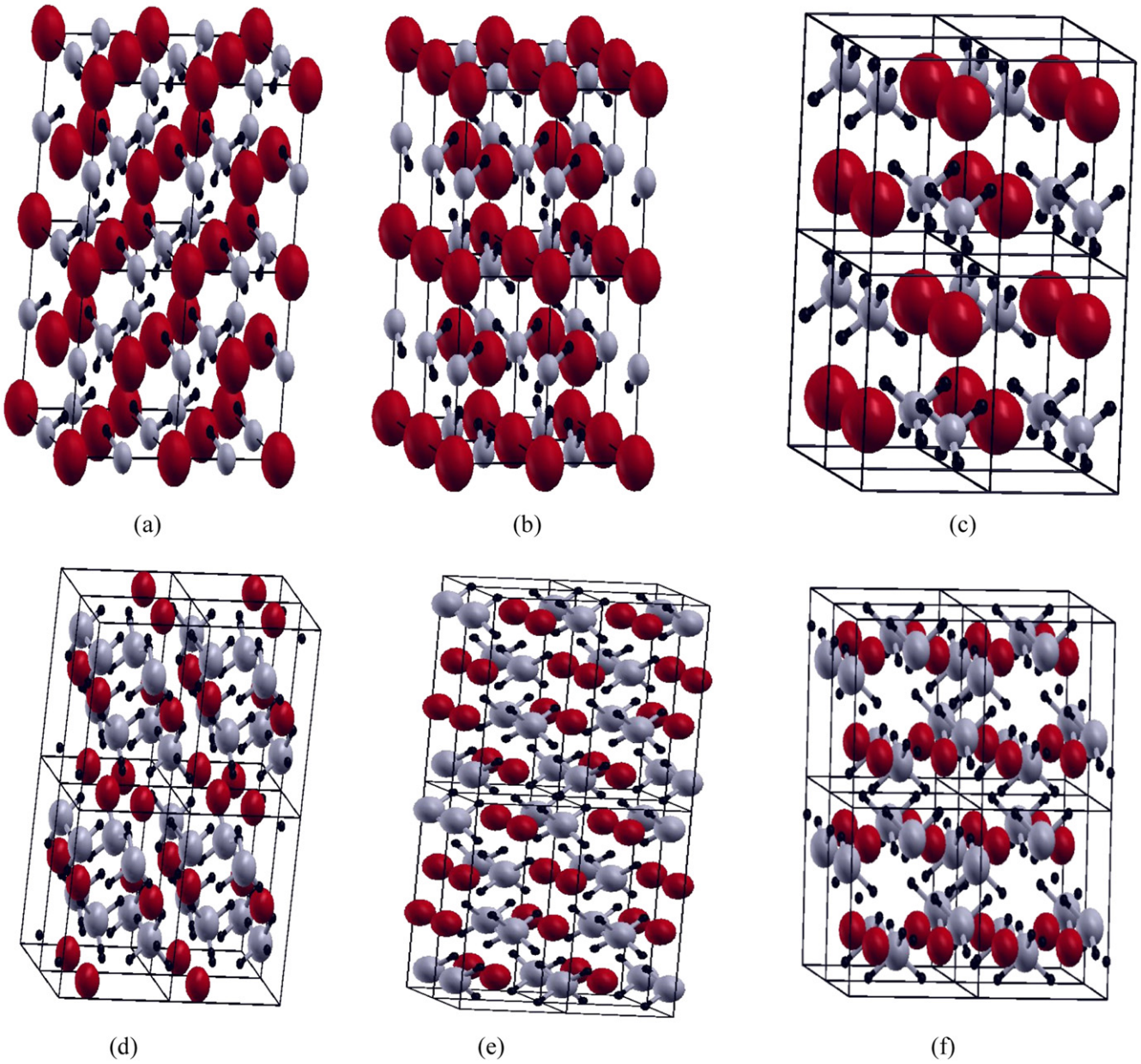

Figure 1. Crystal structure of $NaBH_4$: (a) α phase FCC ($F\bar{4}3m$), (b) β phase tetragonal ($P\bar{4}2_1c$) (c) tetragonal ($P4_2/nmc$) and $LiAlH_4$ structures, (d) α-phase monoclinic ($P2_1/c$), (e) β-phase tetragonal ($I4_1/a$), (f) γ-phase orthorhombic (Pnma). Red: Li–Na; gray: Al–B; black: H.

crystal are related to the reflectivity at normal incidence by [42]

$$R(\omega) = \frac{n + ik - 1}{n + ik + 1} \tag{4}$$

$$I(\omega) = \sqrt{2}\,\omega[\sqrt{\varepsilon_1(\omega)^2 + \varepsilon_2(\omega)^2} - \varepsilon_1(\omega)]^{1/2} \tag{5}$$

$$k(\omega) = I(\omega)/2\omega \tag{6}$$

$$n(\omega) = (1/\sqrt{2})[\sqrt{\epsilon_1(\omega)^2 + \epsilon_2(\omega)^2} + \epsilon_1(\omega)]^{1/2}. \tag{7}$$

For other phases we used similar formulas to calculate the optical functions.

3. Results and discussions

3.1. Total energy calculations and phase stability of $NaBH_4$ and LiAlH4 compounds

Here, we focus our attention on the crystal structure of the technologically important borohydride and analates $NaBH_4$ and $LiAlH_4$ compounds. A comprehensive study of the bonding and structure of these hydrides and their stability is required. For the present work we have investigated six different possible structure types, α-$NaBH_4$ (Fcc; $F\bar{4}3m$), β-$NaBH_4$ (tetragonal; $P\bar{4}2_1c$), γ-$NaBH_4$ (tetragonal; $P4_2/nmc$), α-$LiAlH_4$ (monoclinic; $P2_1/c$), β-$LiAlH_4$ (centered tetragonal; $I4_1/a$) and γ-$LiAlH_4$ (orthorhombic;Pnma) as shown in figure 1.

Table 1. Calculated atomic positions (fractional coordinates) of $NaBH_4$ and $LiAlH_4$ using LDA and GGA.

Compounds	Atomic positions	
	GGA	LDA
α-$NaBH_4$ ($F\bar{4}3m$)	Na: 0, 0, 0	Na: 0, 0, 0
	B: 1/2, 1/2, 1/2	B: 1/2, 1/2, 1/2
	H: 0.3849, 0.3849, 0.3849 (0.3901, 0.3901, 0.3901)[a]	H: 0.38 409, 0.38 409, 0.38 409 (0.3901, 0.3901, 0.3901)[a]
β-$NaBH_4$ ($P\bar{4}2_1c$)	Na: 0, 0, 0	Na: 0, 0, 0
	B: 0, 0, 1/2	B: 0, 0, 1/2
	H: 0.0111, 0.7694, 0.3803 (0.0111, 0.7694, 0.3803)[b]	H: 0.0105, 0.7679, 0.3796 (0.0111, 0.7694, 0.3803)[b]
γ-$NaBH_4$ ($P4_2/nmc$)	Na: 3/4, 1/4, 3/4	Na: 3/4, 1/4, 3/4
	B: 3/4, 1/4, 1/4	B: 3/4, 1/4, 1/4
	H: 1/4, −0.0170, −0.1295 (1/4, −0.0193, −0.1308)[a]	H: 1/4, −0.01 711, −0.12 971 (1/4, −0.0193, −0.1308)[a]
α-$LiAlH_4$ ($P2_1/c$)	Li: 0.5699, 0.4652, 0.8245 (0.5603, 0.4656, 0.8266)[c]	Li: 0.5586, 0.4642, 0.8243 (0.5603, 0.4656, 0.8266)[c]
	Al: 0.1381, 0.2017, 0.9319 (0.1386, 0.2033, 0.9302)[c]	Al: 0.1320, 0.2010, 0.8995 (0.1386, 0.2033, 0.9302)[c]
	H1: 0.1807, 0.0986, 0.7630 (0.1826, 0.0958, 0.7630)[c]	H1: 0.1816, 0.0910, 0.7618 (0.1826, 0.0958, 0.7630)[c]
	H2: 0.3542, 0.3723, 0.9777 (0.3524, 0.3713, 0.9749)[c]	H2: 0.3480, 0.3702, 0.9740 (0.3524, 0.3713, 0.9749)[c]
	H3: 0.2361, 0.0810, 0.1146 (0.2425, 0.0806, 0.1148)[c]	H3: 0.2401, 0.0805, 0.1112 (0.2425, 0.0806, 0.1148)[c]
	H4: 0.7948, 0.2633, 0.8717 (0.7994, 0.2649, 0.8724)[c]	H4: 0.7880, 0.2640, 0.8723 (0.7994, 0.2649, 0.8724)[c]
β-$LiAlH_4$ ($I4_1/a$)	Li: 0, 1/4, 5/8	Li: 0, 1/4, 5/8
	Al: 0, 1/4, 1/8	Al: 0, 1/4, 1/8
	H: 0.2509, 0.5883, 0.5437 (0.2492, 0.4191, 0.5429)[d]	H: 0.2529, 0.5774, 0.5453 (0.2492, 0.4191, 0.5429)[d]
γ-$LiAlH_4$ (Pnma)	Li: 0.2441, 1/4, 0.2469 (0.2428, 1/4, 0.2467)[e]	Li: 0.2454, 1/4, 0.2479 (0.2428, 1/4, 0.2467)[e]
	Al: 0.5097, 1/4, 0, 8186 (0.5120, 1/4, 0, 8221)[e]	Al: 0.5067, 1/4, 0, 8138 (0.5120, 1/4, 0, 8221)[e]
	H1: 0.3023, 1/4, 0.9607 (0.3067, 1/4, 0.9617)[e]	H1: 0.2970, 1/4, 0.9562 (0.3067, 1/4, 0.9617)[e]
	H2: 0.7161, 1/4, 0.9625 (0.7162, 1/4, 0.9631)[e]	H2: 0.7144, 1/4, 0.9580 (0.7162, 1/4, 0.9631)[e]
	H3: 0.4914, 0.0193, 0.2994 (0.4889, 0.9833, 0.2943)[e]	H3: 0.4941, 0.0234, 0.3002 (0.4889, 0.9833, 0.2943)[e]

[a] Experimental values from [43].
[b] DFT [10].
[c] Experimental values from [44].
[d] DFT calculated value at transition point [5].
[e] DFT calculated value at equilibrium [5].

$LiAlH_4$ crystallizes in three different phases, the monoclinic α-$LiAlH_4$-type structure with four formula units per unit cell (24 atoms in a primitive cell), β-$LiAlH_4$ with two formula units per unit cell (12 atoms in a primitive cell) and γ-$LiAlH_4$ with four formula units per unit cell (24 atoms in a primitive cell). $NaBH_4$ can exists in the cubic α-$NaBH_4$-type structure with one formula unit per unit cell (6 atoms in a primitive cell), β-$NaBH_4$ with two formula units per unit cell (12 atoms in a primitive cell) and γ-$NaBH_4$ with two formula units per unit cell (12 atoms in a primitive cell).

The phases are completely relaxed for all volumes in this study using force optimization. The calculated atomic positions for each compound using both LDA and GGA in each phase are presented in table 1 and compared with the available theoretical and experimental data. Calculated data are in good agreement with experiments and previous theoretical works [5, 10, 43, and 44].

The structures of all compounds are optimized by calculating the total energy as a function of volume, then the results are fitted according to the Murnaghan equation of state [45]. The obtained total energy versus volume calculated using LDA and GGA for $NaBH_4$ and $LiAlH_4$ compounds is shown in figure 2. We have studied $NaBH_4$ in the tetragonal phase with two space groups ($P\bar{4}2_1c$) and the higher symmetry ($P4_2/nmc$). It is clearly seen that the low-temperature structure of $NaBH_4$ is β phase, which has ($P\bar{4}2_1c$) symmetry. This is in good agreement with the theoretical calculations carried out by Vajeeston *et al* [10] and Caputo *et al* [25] that predict that at lower temperatures $NaBH_4$ crystallizes in the tetragonal phase, which is consistent with the experimental results [13]. Recently, Kim *et al* [24] found that the tetragonal ($P\bar{4}2_1c$) is the most stable phase at zero temperature and pressure by carrying out Car–Parrinello molecular dynamics simulations. It transforms into a γ phase ($P4_2/nmc$) high-pressure phase at 2.43 GPa. This phase transition is not detected when using the LDA (see figure 2(b)). To be sure, we have also calculated the enthalpy of each phase for $NaBH_4$ and $LiAlH_4$ compounds. The obtained results are shown in figure 2. One can see that no phase transition is observed with the LDA. In the present study, we find that the energy difference between the two phases is only about 12.14 (3.01) meV/formula unit using GGA (LDA), respectively. However, the α phase has high energy so it is considered to be an unstable phase. It was characterized to be a high temperature (200 K) cubic phase by synchrotron diffraction on a $NaBH_4$ single crystal [46]. The transition from the cubic phase to tetragonal phase at 0 GPa occured at 133 K, which is lower than the value of T_c found experimentally (about 190 K) [26]. It was found that on cooling below about 190 K, or under pressure to approximately 6 GPa at ambient temperature, an ordered tetragonal structure appears [47, 48]. The transition from the tetragonal to the cubic phase is

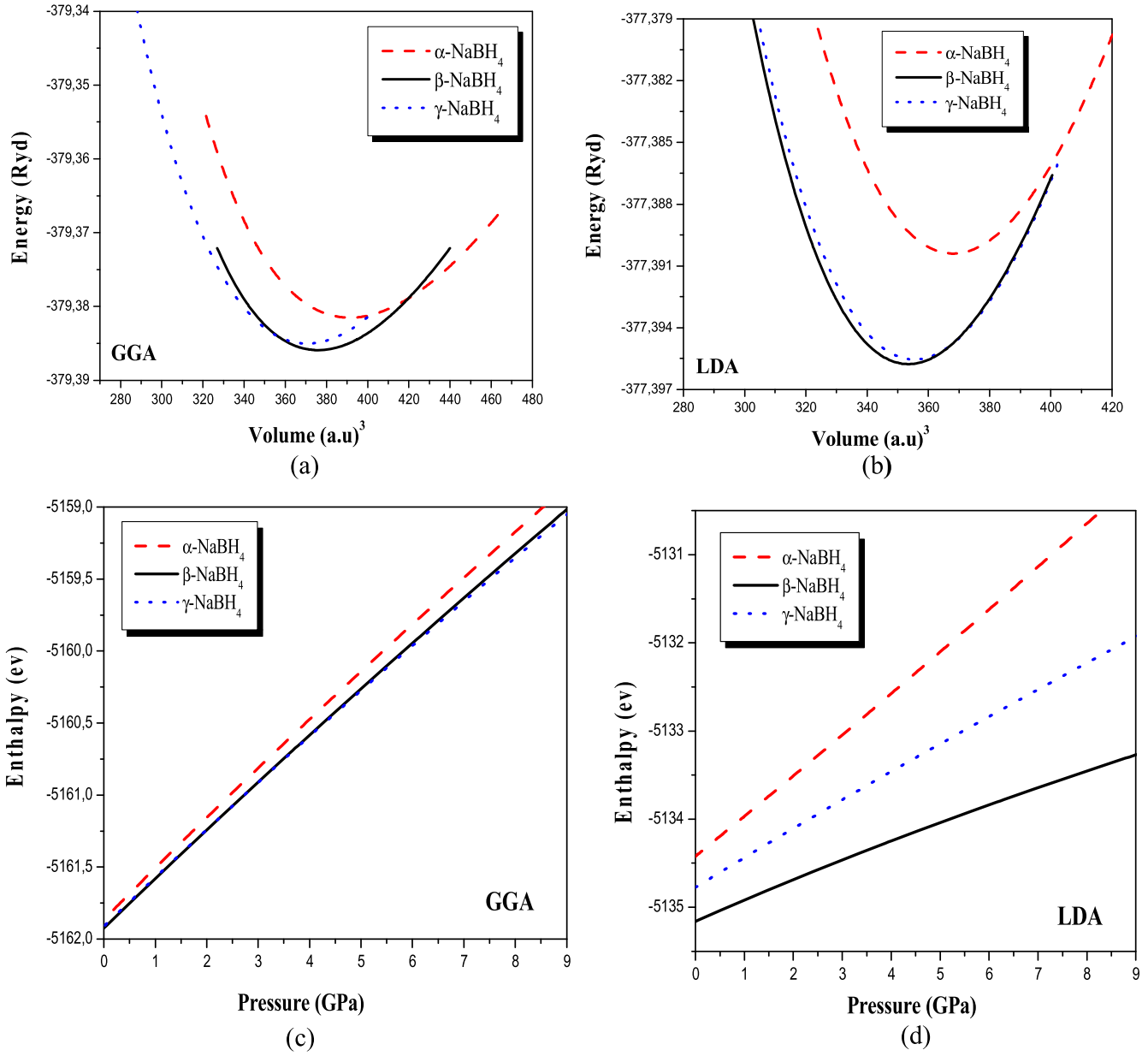

Figure 2. Variation of total energies and total enthalpies as a function of volume and pressure of unit cell, respectively: α phase (dashed curve), β phase (solid curve) and γ phase (dotted curve) using LDA and GGA for: (a), (b), (c) and (d) $NaBH_4$ compound; (e), (f), (g) and (h) $LiAlH_4$ compound.

accompanied by a small volume increase of about 4% (3.45%) calculated using GGA (LDA), respectively.

In the cubic ($F\bar{4}3m$) crystal structure, each $[BH_4]^-$ group is surrounded by six Na^+ atoms and each Na^+ atom by six $[BH_4]^-$ groups, both in octahedral configuration. This is in good agreement with the results reported in [49]. The $[BH_4]^-$ groups in the tetragonal phase (β, γ) are ordered in two different orientations (see figures 1(b) and (c)). While in the cubic phase (α), the non-centrosymmetric model allows the $[BH_4]^-$ anion to be fully ordered. In three phases, Na atoms and $[BH_4]^-$ complexes are octahedrally coordinated. The interatomic distances and the bond angles are presented in table 3.

In the β phase tetragonal ($P\bar{4}2_1c$), bond lengths are found to be 1.224, 2.931–3.073, 4.267, 4.247–4.346, and 2.445 Å for B–H, B–Na, B–B, Na–Na, and Na–H, respectively. The angle H–B–H is found to vary between 109.17° and 110.07°. With increasing pressure from 0–2.43 GPa, B–H, B–Na, and Na–H bonds exhibit a small compression in the range 0.011–0.58%, and all the rest of the bonds exhibit a dilatation, which remain very small. The H–B–H bond angles remain unchanged in this pressure range and are about 109.24°–109.94°.

Our investigation of the cubic structure reveals that the $[BH_4]^-$ group exhibits a nearly ideal tetrahedral geometry. The calculated H–B–H angles, 109.47°, are very close to the ideal tetrahedral angle of 109.5°, and the B–H bond lengths show a narrow spread of about 1.22 Å. The calculated Na–B distances are 3.0724 A°, in good agreement with those reported in [50], 3.065 Å at 200 K. In the tetragonal phase at

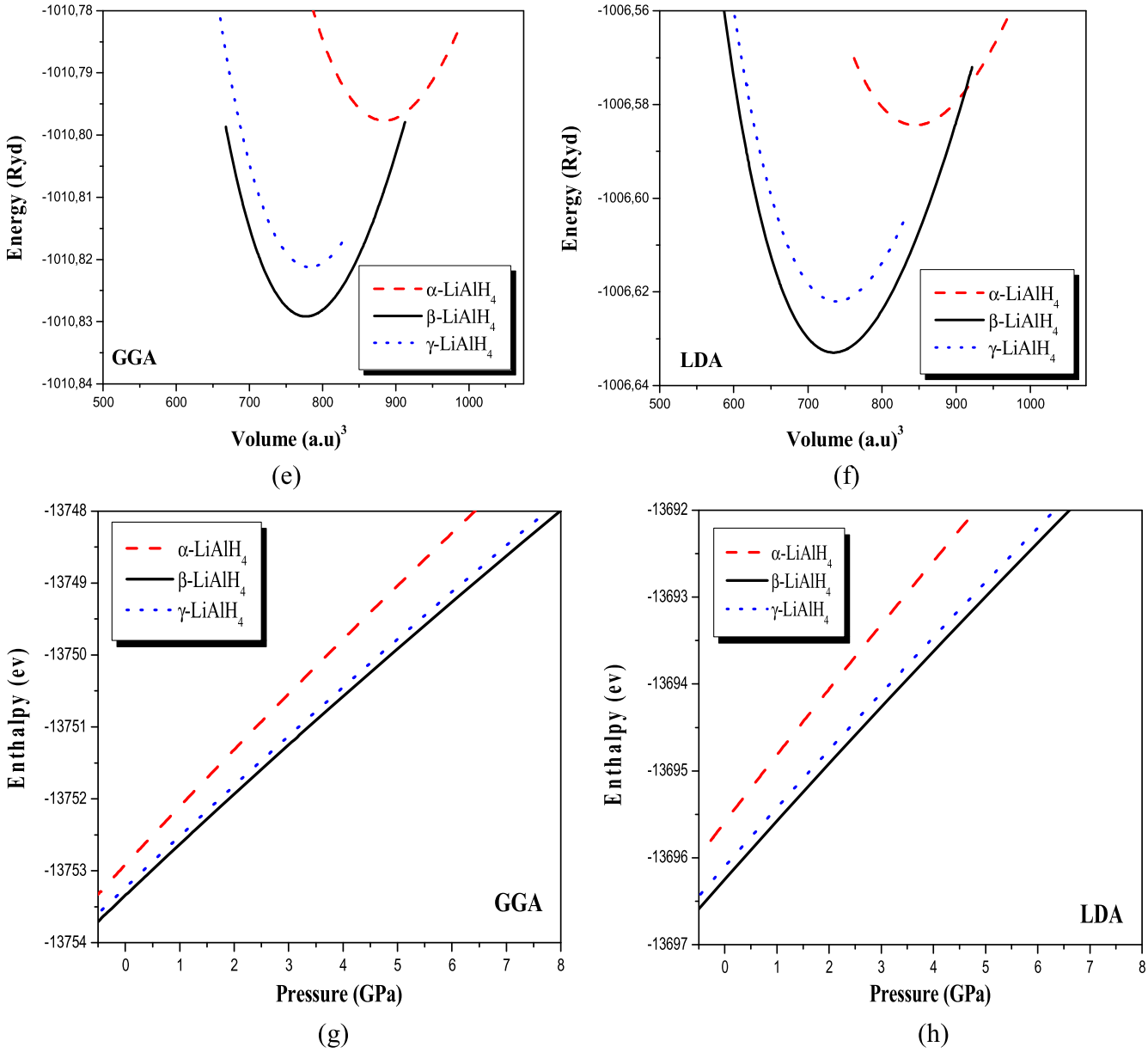

Figure 2. (Continued.)

180 K the bond lengths are about 2.976–3.091 Å. For B–B and Na–H, the bond lengths are found to be 4.3451 Å and 2.568 Å, respectively. It is found that the H–B interactions are of approximately equal strength, whereas the other interactions are slightly different in the three phases.

Our results clearly show that at low temperature the ground state of $LiAlH_4$ is a tetragonal structure (space group $I4_1/a$ (figures 2(e) and (f)) with a slightly different lattice constant a to that of $NaBH_4$, and lattice constant ratio c/a of about 2.25. Our finding is in good agreement with the experimentals results of [51], however it is in disagreement with the results of Vajeeston *et al*, which reported that the most stable phase is the α phase, which transforms to the β phase at 2.6 GPa, accompanied by a large volume decrease of 17% then to the γ phase at 33.8 GPa [5]. It is found that the most stable phase at ambient conditions is the monoclinic α -$LiAlH_4$-type [51]. The calculated energy difference of the two phases, tetragonal and monoclinic, is estimated to be about 59 (73) meV/formula unit using GGA (LDA), respectively. The discrepancy between our results and those of Vajeeston *et al* is due to the method used in calculating the total energy of the system, we used a FP-LAPW method whereas Vajeeston *et al* used the projected augmented plane wave. The Li–H distances ranged from 2.1440 to 3.5171 Å.

The monoclinic α-$LiAlH_4$-type phase with space group $P2_1/c$ and four formula units per unit cell (see figure 1(d)) is a high energy state, as presented in figure 2. It is reported that heating to 360–370 K at ambient pressure produced a transformation from the β phase to the α phase accompanied by a strong endothermal effect [48]. Four hydrogen atoms surrounded aluminum in an almost regular tetrahedral configuration. The phase forms of AlH_4 groups are well

Table 2. Calculated lattice constants (a, b and c) in Å, bulk modulus (B) in GPa and pressure derivative (B') at equilibrium volume using LDA and GGA compared to experimental and other works, of $NaBH_4$ and $LiAlH_4$ for α, β *and* γ phases.

	Lattice constants		B (GPa)			B' (GPa)			Relative error	
Compounds	GGA	LDA	GGA	LDA	Experiment/DFT	GGA	LDA	Experiment/DFT	GGA	LDA
α-$NaBH_4$ ($F\bar{4}3m$)	$a = 6.1449$ (6.148)[a]	$a = 6.02$ (6.148)[a]	42.76	50.87	7.6 [10]	4.91	3.10	5.5 [10]	$\frac{\Delta a}{a}\Big\|_{Exp} = -0.05$	$\frac{\Delta a}{a}\Big\|_{Exp} = -2.12$
					19.9, 18.76 [24, 47]			3.5, 3.48 [24, 47]		
β-$NaBH_4$ ($P\bar{4}2_1c$)	$a = 4.3553$ (4.3464)[b]	$a = 4.2743$ (4.3464)[b]	49.06	53.60	7.8 [10]	4.41	3.1	5.4 [10]	$\frac{\Delta a}{a}\Big\|_{DFT} = 0.20$	$\frac{\Delta a}{a}\Big\|_{DFT} = -1.68$
	$c = 5.8740$ (5.8620)[b]	$c = 5.7648$ (5.8620)[b]							$\frac{\Delta c}{c}\Big\|_{DFT} = 0.20$	$\frac{\Delta c}{c}\Big\|_{DFT} = -1.68$
	$c/a = 1.35$	$c/a = 1.35$								
γ-$NaBH_4$ ($P4_2/nmc$)	$a = 4.3277$ (4.3320)[a]	$a = 4.2634$ (4.3320)[a]	50.18	52.80	20.1 [10]	3.22	2.41	4.5 [10]	$\frac{\Delta a}{a}\Big\|_{DFT} = -0.09$	$\frac{\Delta a}{a}\Big\|_{DFT} = -1.60$
	$c = 5.8675$ (5.8690)[a]	$c = 5.7761$ (5.8690)[a]							$\frac{\Delta c}{c}\Big\|_{DFT} = -0.02$	$\frac{\Delta c}{c}\Big\|_{DFT} = -1.60$
	$c/a = 1.355$	$c/a = 1.354$								
α-$LiAlH_4$ ($P2_1/c$)	$a = 4.6363$ (4.8174)[c]	$a = 4.5660$ (4.8174)[c]	42.03	44.68	12.95 [5]	2.75	3.43	4.10 [5]	$\frac{\Delta a}{a}\Big\|_{DFT} = -3.90$	$\frac{\Delta a}{a}\Big\|_{DFT} = -5.50$
	$b = 7.5551$ (7.8020)[c]	$b = 7.3948$ (7.8020)[c]			12.9 [52]			4.10 [52]	$\frac{\Delta b}{b}\Big\|_{DFT} = -3.26$	$\frac{\Delta b}{b}\Big\|_{DFT} = -5.50$
	$c = 7.5737$ (7.8214)[c]	$c = 7.4132$ (7.8214)[c]							$\frac{\Delta c}{c}\Big\|_{DFT} = -3.27$	$\frac{\Delta c}{c}\Big\|_{DFT} = -5.50$
	$\beta = 111.858$ (112.228)[c]	$\beta = 111.852$ (112.228)[c]								
	$b/a = 1.629$	$b/a = 1.619$								
	$c/a = 1.633$	$c/a = 1.623$								
β-$LiAlH_4$ ($I4_1/a$)	$a = 4.6675$ (4.7312)[d]	$a = 4.5809$ (4.7312)[d]	47.75	51.87	25.64 [5]	2.86	3.33	4.35 [5]	$\frac{\Delta a}{a}\Big\|_{DFT} = -1.36$	$\frac{\Delta a}{a}\Big\|_{DFT} = -3.28$
	$c = 10.5253$ (10.7161)[d]	$c = 10.3298$ (10.7161)[d]			25.64 [53]			4.35 [53]	$\frac{\Delta c}{c}\Big\|_{DFT} = -1.81$	$\frac{\Delta c}{c}\Big\|_{DFT} = -3.73$
	$c/a = 2.255$	$c/a = 2.254$								
γ-$LiAlH_4$ (Pnma)	$a = 6.5023$ (6.4667)[e]	$a = 6.3787$ (6.4667)[e]	48.90	52.69	14.25 [5]	3.02	3.15	4.85 [5]	$\frac{\Delta a}{a}\Big\|_{DFT} = 0.54$	$\frac{\Delta a}{a}\Big\|_{DFT} = -1.37$
	$b = 5.4097$ (5.3478)[e]	$b = 5.4026$ (5.3478)[e]							$\frac{\Delta b}{b}\Big\|_{DFT} = 1.14$	$\frac{\Delta b}{b}\Big\|_{DFT} = 1.01$
	$c = 6.5968$ (6.5931)[e]	$c = 6.4396$ (6.5931)[e]							$\frac{\Delta c}{c}\Big\|_{DFT} = 0.05$	$\frac{\Delta c}{c}\Big\|_{DFT} = -2.38$
	$b/a = 0.832$	$b/a = 0.846$								
	$c/a = 1.014$	$c/a = 1.009$								

[a] Experimental values from [43].
[b] DFT [10].
[c] Experimental values from [44].
[d] DFT calculated value at transition point [5].
[e] DFT calculated value at equilibrium [5].

Table 3. Selected interatomic distances (Å) and angles (deg) in various crystal structures.

Compounds	Phases	Atoms	Our calculation	Experiment, 8K [24]
$LiAlH_4$	α-$LiAlH_4$	Al–H_1	1.555	1.625
		Al–H_2	1.553	1.621
		Al–H_3	1.548	1.645
		Al–H_4	1.537	1.596
		Li–H_1	1.807	1.896
		Li–H_2	1.912	1.932
				1.978
		Li–H_3	1.714	1.841
		Li–H_4	1.789	1.870
		Li–Al	3.017	3.200
			3.077	3.232
			3.139	3.265
			3.232	3.285
				3.401
		H_1–Al–H_2	110.498	109.0
		H_1–Al–H_3	107.083	108.2
		H_1–Al–H_4	110.515	111.0
		H_2–Al–H_3	109.016	108.9
		H_2–Al–H_4	107.119	108.4
		H_3–Al–H_4	112.544	111.3
		Li–Li	3.749	
		Al–Al	3.849	
	β-$LiAlH_4$	Al–H (×4)	1.628	
		Li–H	2.144	
		Li–Al (×2)	3.300	
		Li–Al (×3)	3.517	
		H–Al–H (×2)	106.018	
		H–Al–H (×2)	116.623	
		Li–Li	3.517	
		Al–Al	3.517	
	γ-$LiAlH_4$	Al–H_1 (×2)	1.652	
		Al–H_2 (×1)	1.643	
		Al–H_3 (×1)	1.643	
		Li–H	2.065	
		Li–Al	3.172	
		H_1–Al–H_2	105.374	
		H_1–Al–H_2	106.036	
		H_1–Al–H_3	109.897	
		H_2–Al–H_3	123.753	
		Li–Li	3.251	
		Al–Al	3.375	
	α-$NaBH_4$	B–H (×4)	1.2248	1.19 at 200° K [46]
		Na–H (×8)	2.5680	
$NaBH_4$		B–Na (×6)	3.07 245	
		H–B–H (×4)	109.471	
		B–B (×12)	4.345	
		Na–Na (×12)	4.345	
	β-$NaBH_4$	B–H (×4)	1.227	1.22 at 10 K [43]
		Na–H (×4)	2.448	2.44 at 10 K [43]
		Na–H (×4)	2.531	2.59 at 10 K [43]
		B–Na (×4)	3.079	3.091 at 180 K [46]
		B–Na (×2)	2.9370	2.976 at 180 K [46]
		H–B–H (×2)	109.172	
		H–B–H (×2)	110.072	
		B–B (×8)	4.2556	
		Na–Na (8)	4.256	
	γ-$NaBH_4$	B–H (×4)	1.231	
		Na–H (×4)	2.445	
		Na–H (×4)	2.553	

Table 3. (Continued.)

Compounds	Phases	Atoms	Our calculation	Experiment, 8K [24]
		B–Na (×4)	3.060	
		B–Na (×2)	2.934	
		H–B–H (×2)	109.238	
		H–B–H (×2)	109.939	
		B–B (×8)	4.239	
		Na–Na (×4)	4.239	
		Na–Na (×4)	4.328	

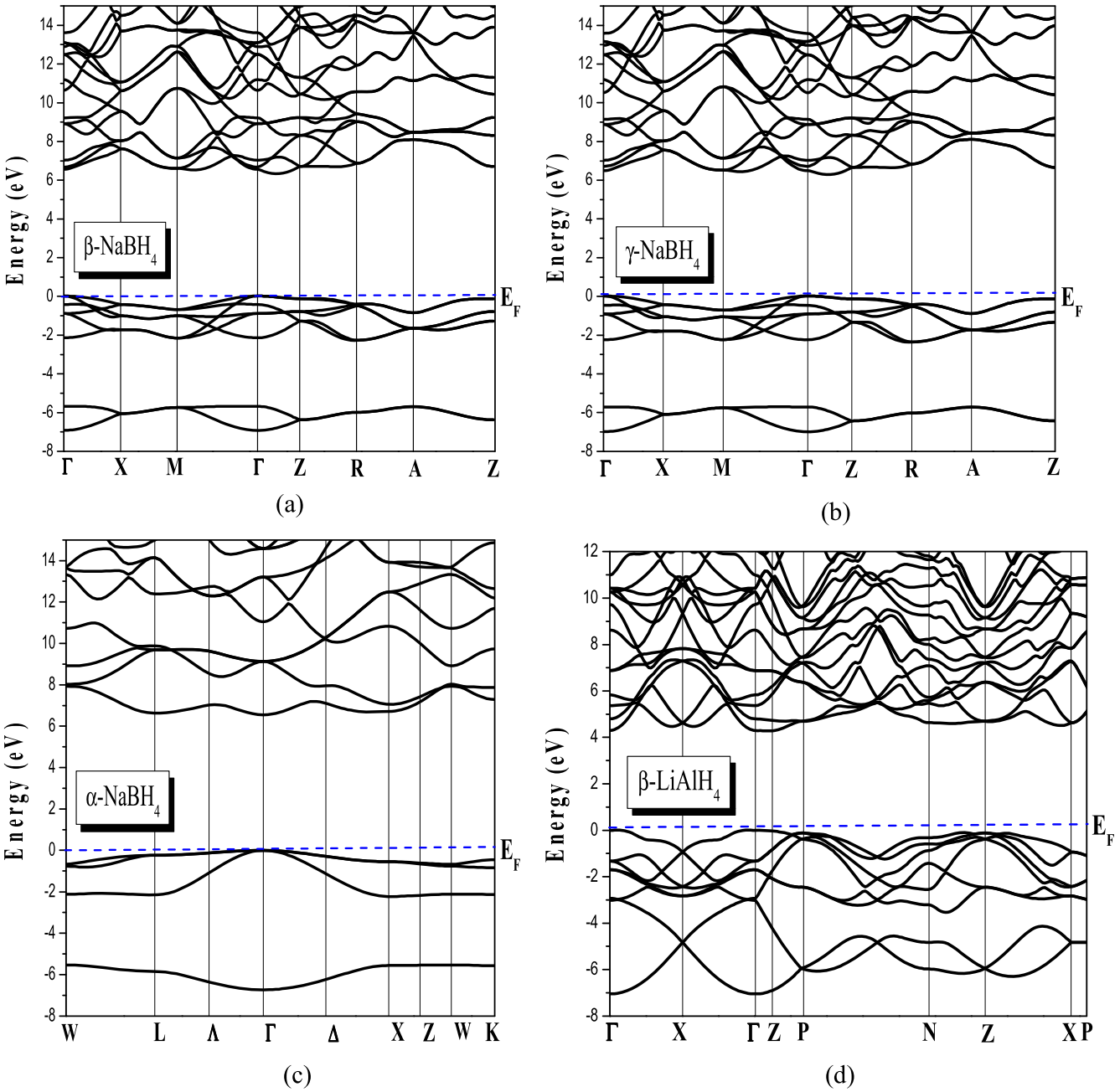

Figure 3. Band structure along the symmetry lines of the BZ for $NaBH_4$: (a) β-$NaBH_4$ (primitive tetragonal; $P\bar{4}2_1c$), (b) γ-$NaBH_4$ (primitive tetragonal; $P4_2/nmc$) and (c) α-$NaBH_4$ (FCC cubic; $F\bar{4}3m$). For $LiAlH_4$: (d) β-$LiAlH_4$ (centered tetragonal; $I4_1/a$), (e) γ-$LiAlH_4$ (primitive orthorhombic; Pnma) and (f) α-$LiAlH_4$ (primitive monoclinic; $P2_1/c$). The position of the Fermi level is shown by the horizontal line.

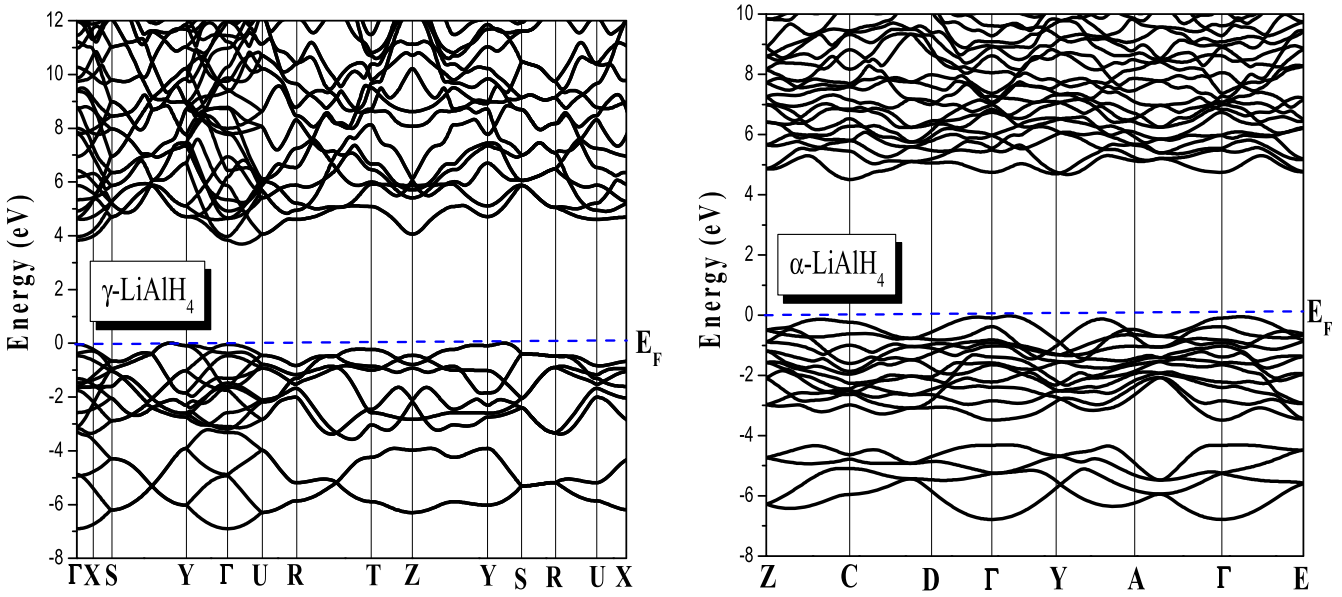

Figure 3. (Continued.)

separated by Li ions. The Al–H distances vary between 1.548 and 1.555 Å, the Li–H separations between 1.71 and 1.91 Å, and the arrangement of the lithium ions leads to a Li–Li distance of about 3.75 Å. The minimum Al–Al distance between tetrahedra is 3.849 Å, greater than that reported in [6] of about 3.754 Å at 295 K. The H–Al–H angles of $LiAlH_4$ are found to vary by less than 2.5° from the angles of a perfect tetrahedron.

Between these two structures, we obtained the orthorhombic structure where each Al has four H tetrahedrally coordinated forming a stable complex of $[AlH_4]^-$ with Al–H bond lengths of 1.64–1.65 Å. The minimum Al–Al distance between the tetrahedra was 3.37 Å. In addition, H–Al–H bond angles were close to ideal and ranged from 105.4 to 109.9° except one which is about 123.75°. Furthermore, the minimum Li–H separation was 2.06 Å, larger than that in the α phase and shorter than that of the β phase. However, we find that the total energy is 7.940 (10.938) mRy) calculated by GGA (LDA), respectively, per formula unit higher than that of the tetragonal phase. The transition from the tetragonal to the monoclinic structure is accompanied by the large volume increase of about 10% (11.19%) calculated using GGA (LDA), respectively. One can note that the computed $\left.\frac{\Delta a}{a}\right|_{Exp}$ shows that the deviation of lattice parameter from experiment calculated by GGA is less than that calculated using LDA (see table 2). So we conclude that the GGA is a good approximation for bonding properties for this kind of hydride.

The most commonly used equation of states (EoS) for fitting the isothermal P–V datasets are due to Murnaghan and Birch. Assuming that the bulk modulus varies linearly with pressure $B = B_0 + P$, B'_0, where B'_0 is independent of pressure, the Murnaghan EoS [45] can be derived. The bulk modulus B_0 of the β phase of $NaBH_4$ is found to be 49.06 (53.60) GPa with its pressure derivative $B'_0 = 4.41$ (3.15) and equilibrium unit cell volume $V_o = 54.95$ (52.50) Å^3 using GGA (LDA). The bulk modules of $NaBH_4$ and $LiAlH_4$ in the studied phases are higher than all other reported values [5, 10, 24, 47, 52, 53].

It is interesting to note that the studied compounds have bulk modulus in the same range of about 50 GPa and they are easily compressible. The soft nature of these materials is due to the ionic bonding between Na^+ (Li^+) and the $[XH_4]^-$ complexes, although there exists strong covalent bonding between H and X in the $[XH_4]^-$ complexes.

From table 2, it is shown that the bulk modulus of $NaBH_4$, found by LDA or GGA, is higher than that of $LiAlH_4$ in all phases α, β and γ, suggesting that Na atoms induced hardening of this material. The lower bulk modulus (high compressibility) observed for $LiAlH_4$ as compared to the corresponding $NaBH_4$ could be due to partial charge transfer between Na and BH_4. Generally, borohydrides are more stable than alanates, and their stability also increases with the increase in atomic number of alkali metals. Our values of the bulk modulus ranged between 40 and 50 GPa, which suggests possible destabilization under pressure. No high-pressure phase transition in $LiAlH_4$ from α to β then to γ phase at 0 K is detected in our calculations using both GGA and LDA (figure 2).

3.2. Electronic band structure and density of states

The self-consistent scalar relativistic band structures of $NaBH_4$ and $LiAlH_4$ compounds along representative

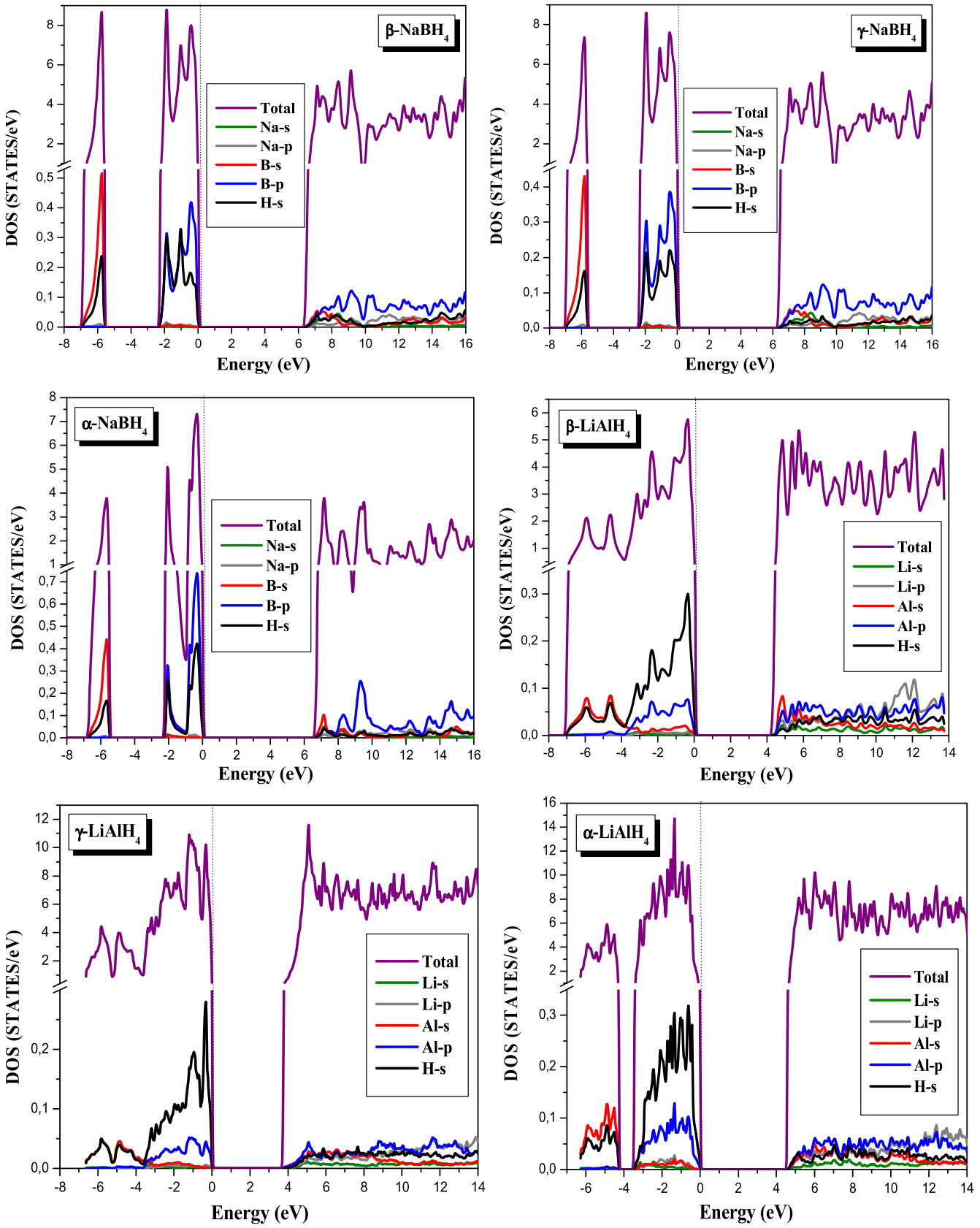

Figure 4. The calculated total and partial DOS for $NaBH_4$ and $LiAlH_4$ in the β, γ and α phases. The graph is scaled for 0 eV at the Fermi level (E_F).

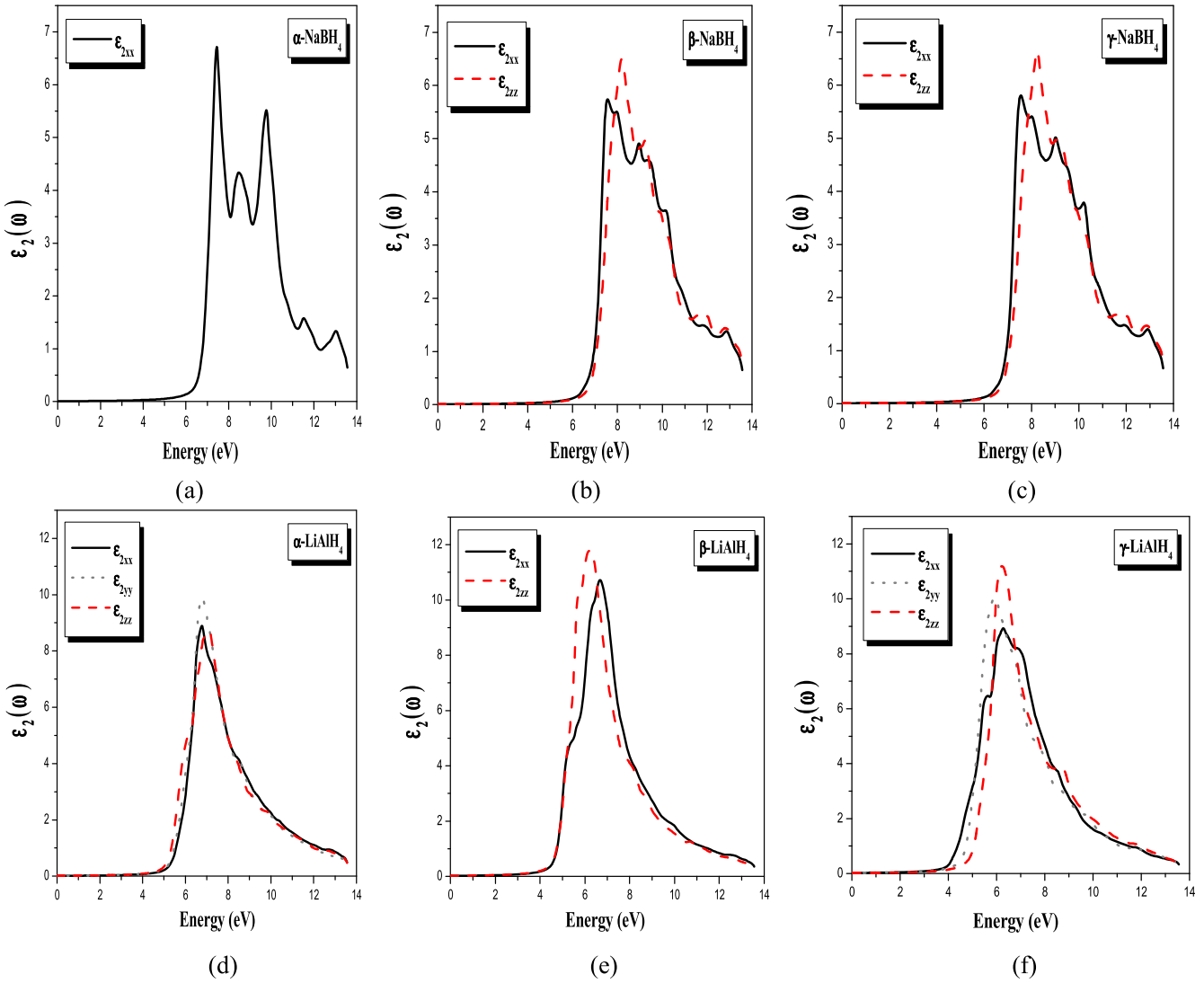

Figure 5. The imaginary part $\varepsilon_2(\omega)$ of the dielectric functions for $NaBH_4$ ((a), (b) and (c)) and for $LiAlH_4$ (d), (e) and (f)).

Table 4. Calculated $\varepsilon_1(0)$ and E_g of $NaBH_4$ and $LiAlH_4$ compounds within LDA, GGA and EV-GGA.

	E_g (eV)				$\varepsilon_1(0)$			
Compounds	GGA	LDA	EV-GGA	Other calculations		GGA	LDA	EV-GGA
α-$NaBH_4$	6.548	6.232	7.552	6 [29], 6.5 [10]	ε_{1xx}	241 988	261 559	205 436
β-$NaBH_4$	6.415	6.089	7.633	6 [29], 6.5 [10]	ε_{1xx}	245 059	263 8189	205 069
					ε_{1zz}	240 192	257 721	200 928
γ-$NaBH_4$	6.375	6.079	7.603		ε_{1xx}	247631	264 5699	207 199
					ε_{1zz}	242 457	258 341	202 925
α-$LiAlH_4$	4.567	3.780	6.152	4.71 [5], 4.8 [56], 4.77 [57], 4.19 [57], 4.67 [57]	ε_{1xx}	312 591	353 3137	242 721
					ε_{1yy}	321 991	364 981	247 991
					ε_{1zz}	323 67	366 224	249 646
β-$LiAlH_4$	4.276	3.768	5.799	4.25 [5]	ε_{1xx}	384 518	425 358	286 687
					ε_{1zz}	400 426	4485	294 466
γ-$LiAlH_4$	3.756	3.194	5.119	3.95 [5]	ε_{1xx}	389 724	439 504	288 791
					ε_{1yy}	38 602	435 508	285 668
					ε_{1zz}	364 977	40 347	276 212

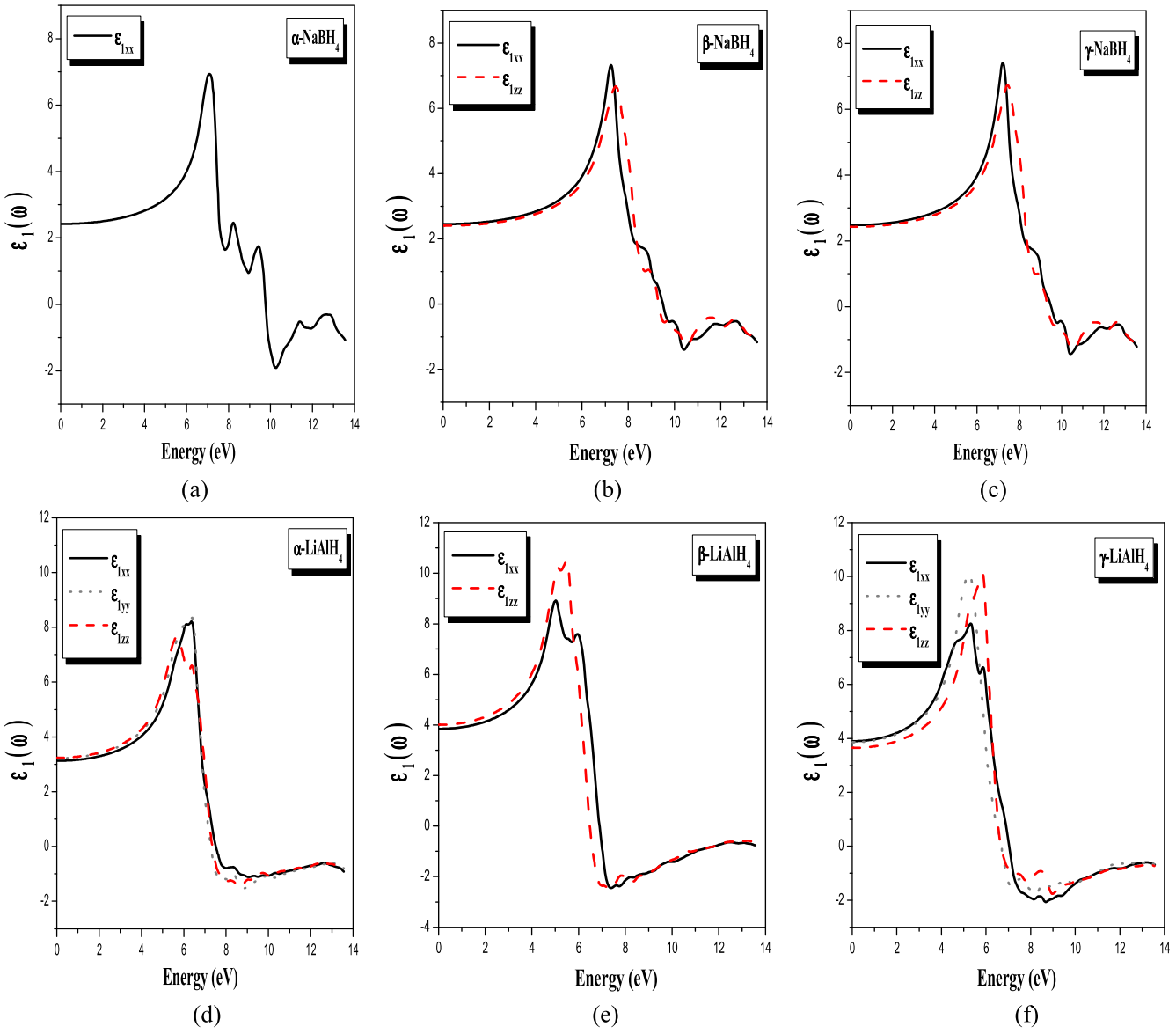

Figure 6. Real parts of dielectric functions for $NaBH_4$ ((a), (b) and (c)) and for $LiAlH_4$ ((d), (e) and (f)).

symetrical directions of the Brillouin zone were obtained at equilibrium volume as well as at far from equilibrium within the LDA and GGA. The Fermi level E_F is shown by a dashed horizontal line in figure 3.

We have also shown the band structure of $NaBH_4$ and $LiAlH_4$ compounds in the α, β and γ phases in figure 3. From the graphs, the gap between the valence and conduction bands is calculated using GGA and LDA to be between 3 eV and 6.5 eV, which gives $NaBH_4$ and $LiAlH_4$ compounds the property of being a large band gap insulating material. It is noted that the dispersions of bands in β- and γ-$NaBH_4$ phases are very similar. The valence band maximum is at the Γ point and the conduction band minimum is located in the Γ–Z direction for β- and γ-$NaBH_4$ phases. The band structure of α-$NaBH_4$ is qualitatively different and shows a direct band gap at the Γ point. The picture is quite different for $LiAlH_4$; it shows a direct band gap at the Γ point in the β-$LiAlH_4$ phase. For the monoclinic (phase α), $LiAlH_4$ is an indirect band gap material with a gap in the direction Γ–C, while in the phase γ-$LiAlH_4$, the valence band maximum is located in the S–Y direction and the conduction band minimum is located in the Γ–U direction, which causes an indirect band gap.

The total and partial density of states of $NaBH_4$ and $LiAlH_4$ compounds are presented in figure 4. There is a hybridization between the H and the B-s and B-p states in the valence bands, with the lowest valence bands having some B-s and the highest having some B-p character, respectively. The conduction bands have a mixed Na, B and H character in the three phases of $NaBH_4$. The LDOS on the B, Na and H atoms is very similar in β- and γ- $NaBH_4$, but there are small differences in the α phase in $NaBH_4$. In $LiAlH_4$ there is a large contibution of H states in the highest valence bands, however in the lowest ones the Al-s states donimate in the α phase. It is clearly seen that the disappearance of the gap

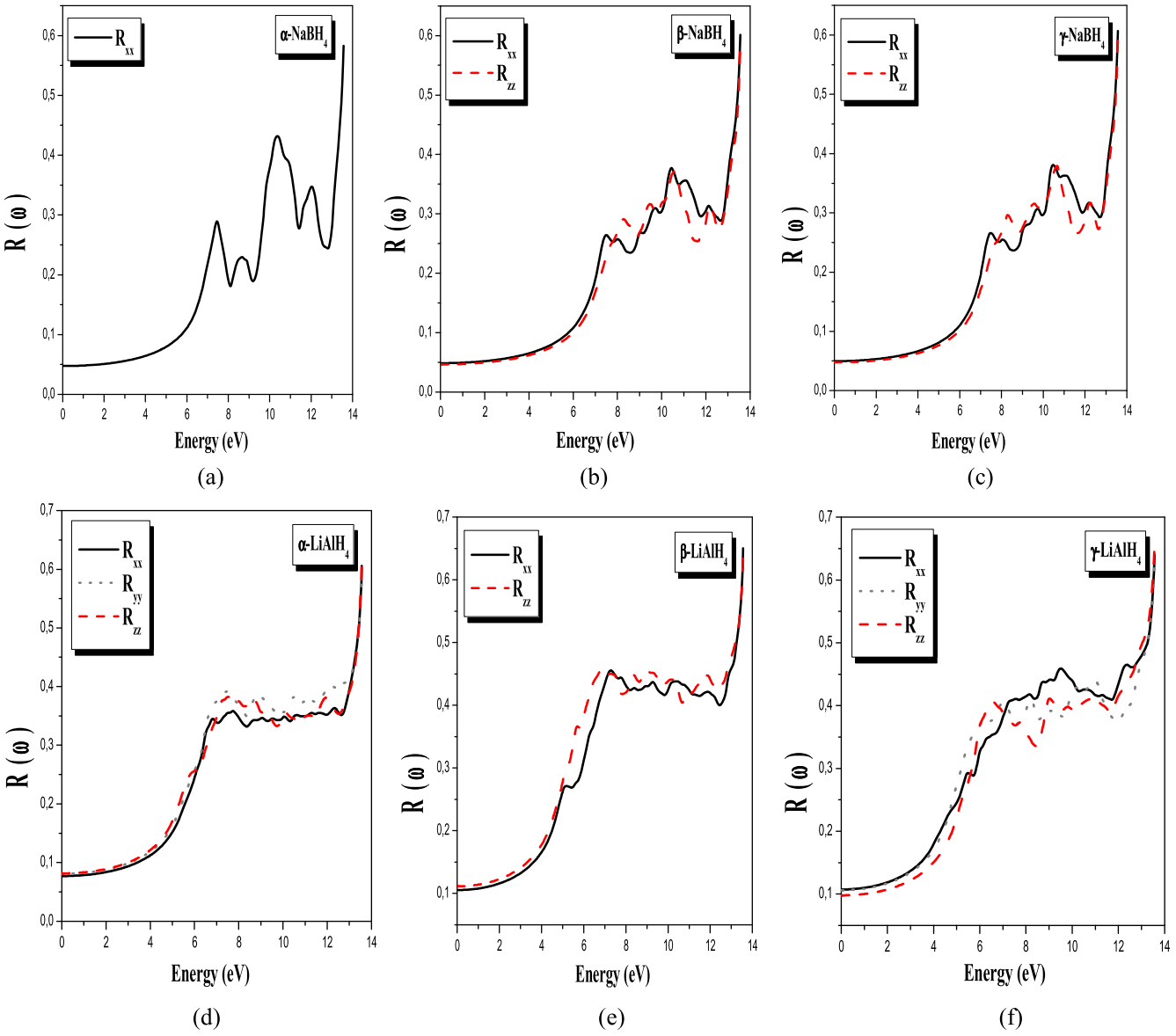

Figure 7. Calculated reflectivity $R(\omega)$ and $I(\omega)$, the absorption coefficient in 10^4 cm^{-1}, of $NaBH_4$ and $LiAlH_4$ in α, β and γ phases.

between the lowest and highest valence bands in the β- and γ-$LiAlH_4$ phase. The valence bands near the Fermi level have a dominant hydrogen character.

Modern DFT provides an extremely valuable tool for predicting structures and energetics of new materials for both finite and periodic systems. DFT calculations generally give good results for ground state properties, but not for excited states. In particular, the band gap in semiconductors and insulators is generally found to be too small when compared with experiment, for instance, it can be underestimated by about 50%. This is mainly because LDA and GGA have simple forms that are not sufficiently flexible for accurately reproducing both exchange-correlation energy (E_{xc}) and its charge derivative. The PBE-GGA is the standard parameter-free GGA, while the EV-GGA has been designed by optimizing the exchange potential rather than using (E_{xc}) [36]. The reason for carrying out calculations using both GGA and EV-GGA is that the EV-GGA has been shown in several cases to give band gaps in good agreement with experiment [54, 55]. The band structure calculated using the GGA and the EV-GGA for the compounds under consideration was similar except for the value of the band gap which was higher within the EV-GGA. The band gap values are listed in table 4, compared with available theoretical works [5, 10, 26, 56, 57], and generally speaking they are close to each other.

3.3. Optical properties

The optical properties of solids provide an important tool for studying energy band structure, lattice vibrations, excitons, impurity levels, localized defects and certain magnetic excitations. The linear optical properties are determined by the complex dielectric function $\varepsilon(\omega) = \varepsilon_1(\omega) + i\varepsilon_2(\omega)$, describing the polarization response of the system to an external electromagnetic field with a small wavevector. The

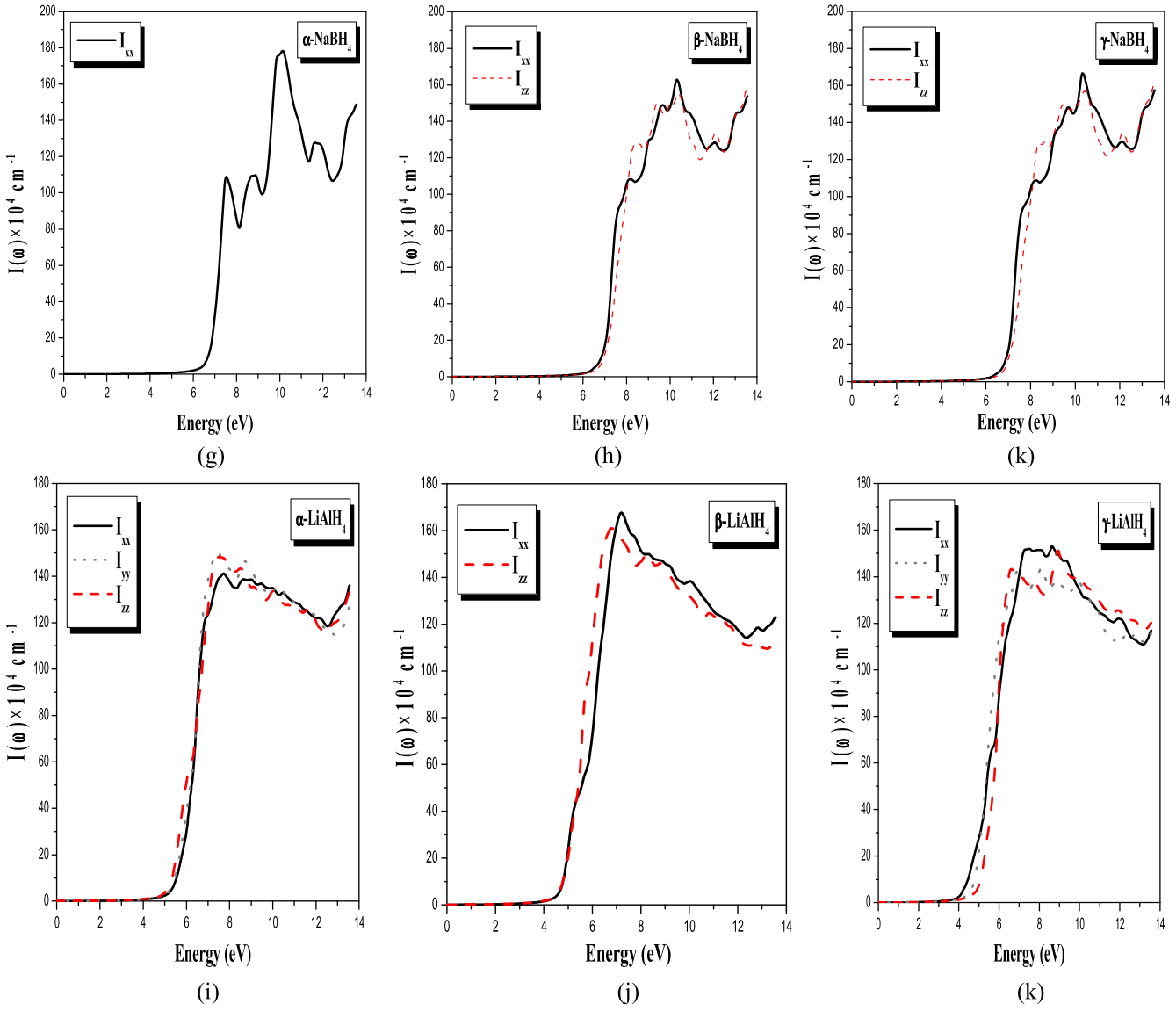

Figure 7. (Continued.)

electric field of the photon leads to the transition between occupied and unoccupied wavevector states [42].

The frequency dependence of a given material is a superposition of the various mechanisms at work in this material. In the idealized case of a model material, all four basic mechanisms in their pure form: interfacial polarization, orientation of permanents dipoles polarization, uonic polarization, and electronic polarization exist. Our compounds are crystalline solids with partially ionic bonding, so there is no contribution to the the dielectric functions from the two polarizations interfacial and orientational.

In our calculations of the imaginary part of the dielectric functions $\varepsilon_2(\omega)$, we neglect the ionic polarization assuming that the real function $\varepsilon_1(\omega)$, calculated using a Kramers–Kronig transformation at low frequencies, is not affected (the relative error is very small).

The cubic symmetry (α-$NaBH_4$ phase) allows one non-zero component of the second-order dielectric (optical) tensor corresponding to the electric field $\vec{E}$ being directed along ***c***-crystallographic axes where the high-pressure phase β and the γ-$NaBH_4$ and β-$LiAlH_4$ phases allow two non-zero components, namely $\varepsilon_2^{\parallel}(\omega)$ and $\varepsilon_2^{\perp}(\omega)$, to completely characterize the linear optical properties. These are the imaginary parts of the frequency dependent dielectric function. The orthorhombic symmetry (γ-$LiAlH_4$ phase) gives rise to three components of the dielectric functions $\varepsilon_2^{xx}(\omega)$, $\varepsilon_2^{yy}(\omega)$ and $\varepsilon_2^{zz}(\omega)$. For monoclinic ($P2_1/c$) symmetry, there are four components $\varepsilon_2^{xx}(\omega)$, $\varepsilon_2^{yy}(\omega)$, $\varepsilon_2^{zz}(\omega)$ and $\varepsilon_2^{xy}(\omega)$, while the xy component is very small so we will not present it here.

Figure 5 illustrates the variation of the imaginary part $\varepsilon_2(\omega)$ of the frequency dependent dielectric function for $NaBH_4$ and $LiAlH_4$ compounds for all the studied phases. The similarity between the band structures of β- and γ-$NaBH_4$ phases gives rise to the same dielectric functions with the same direct optical gap of about 4.44 eV, as is shown in figure 5. It is found that the parallel $\varepsilon_2^{\parallel}(\omega)$ and the

perpendicular $\varepsilon_2^{\perp}(\omega)$ components of the frequency dependent dielectric function show a large anisotropy. We should emphasize that both $\varepsilon_2^{\parallel}(\omega)$ and $\varepsilon_2^{\perp}(\omega)$ display one major peak at around 8.24 and 5.6 eV for the β phase, and at 7.5 and 6.6 eV for $\varepsilon_2^{\parallel}(\omega)$ and $\varepsilon_2^{\perp}(\omega)$ for γ-NaBH4, respectively. There are some humps located on the right shoulders of the main pack of $\varepsilon_2^{\perp}(\omega)$ and $\varepsilon_2^{\parallel}(\omega)$ for β- and γ-$NaBH_4$ phases.

The main peak in the spectrum of $\varepsilon_2^{\perp}(\omega)$ arises from transitions at *R*, near Γ and in $\varepsilon_2^{\parallel}(\omega)$ in transitions near Z. The optical spectrum of $NaBH_4$ in α phase has more structures. The onset is at about 4.42 eV and the main peak is at energy 7.47 eV and the second one is at 5.47 eV.

In the three phases of $LiAlH_4$, the dielectric functions sharply rise above 4–5 eV and reaches its height between 6 and 7 eV. The maximal dielectric response of $LiAlH_4$ in α phase is somewhat smaller than that of β and γ phases, but the shape of the α and γ spectra is notably similar.

The real part of dielectric function is obtained from the imaginary part $\varepsilon_2(\omega)$ by means of a Kramers–Kronig transformation [58] as shown in figures 6(a)–(f). The computed static dielectric constants $\varepsilon_1(0)$ are displayed in table 4.

From figure 6, we can see a large anisotropy in the real part $\varepsilon_1(\omega)$ of the dielectric function for the two compounds near the main peak. Furthermore, $LiAlH_4$ shows a larger high frequency dielectric constant than that of $NaBH_4$ in all phases. This fact is explained by the Penn model $\varepsilon_1(0) \approx 1 + \left(\frac{\hbar\omega p}{E_g}\right)^2$ [59]; the band gap of $NaBH_4$ is larger than that of $LiAlH_4$.

Using the obtained imaginary and real parts of the - frequency dependent dielectric function one can estimate other optical properties such as absorption coefficient $I(\omega)$ and reflectivity spectra $R(\omega)$. According to figure 7, one observes that at low energies these hydrids possess small reflectivity. It starts at 5% for $NaBH_4$ and about 10% for $LiAlH_4$ then a rapid increase in the reflectivity occurs at intermediate and high energies. The strong reflectivity maximum occurs at higher energies around 13.5 eV for $NaBH_4$ and $LiAlH_4$ in all phases. The reflectivity maximum arises from interband transitions. The absorption coefficients of $NaBH_4$ and $LiAlH_4$ in all phases are presented at figures 7(j)–(k). We note that at low energies the absorption coefficient increases drastically to reach its maximum value at higher energies.

4. Conclusions

We have used first principles total energy calculations to study the structure, bonding, electronic structure and optical properties for several phases of $NaBH_4$ and $LiAlH_4$ compounds. The obtained results predict that the materials under consideration crystallize in the tetragonal phase at lower temperatures, which is in agreement with the experimental results. The studied compounds are easily compressible; their bulk moduli are in the same range at about 50 GPa. The soft character of the $NaBH_4$ and $LiAlH_4$ materials is due to the ionic bonding between Na^+ (Li^+) and the $[BH_4]^-$ ($[AlH_4]^-$) units. In addition the obtained bulk modulus of $NaBH_4$ is higher than that of $LiAlH_4$ in all phases α, β and γ, suggesting that Na atoms induced hardening of the material. The DOS shows that the studied compounds display insulating behavior with wide band gaps ranging between 5 and 7.7 eV using the EV-GGA approximation. A large anisotropy in the real part $\varepsilon_1(\omega)$ and imaginary part $\varepsilon_2(\omega)$ of the dielectric function for the two compounds near the main peak is noticed. The reflectivity spectra and absorption coefficient are also calculated and discussed.

References

[1] Schlapbach L and Zuttel A 2001 *Nature* **414** 353
[2] Li C, Peng P, Zhou D W and Wan L 2011 *Int. J. Hydrogen Energy* **36** 14512
[3] Zaluski L, Zaluska A and Ström-Olsen J O 1999 *J. Alloys Compds.* **290** 71
[4] Talyzin A V, Andersson O, Sundqvist B, Kurnosov A and Dubrovinsky L 2007 *J. Sol. Stat. Chem.* **180** 510
[5] Vajeeston P, Ravindran P, Vidya R, Fjellvag H and Kjekshus A 2003 *Phys. Rev.* B **68** 212101
[6] Orimo S, Nakamori Y, Eliseo J R, Züttel A and Jensen C M 2007 *Chem. Rev.* **107** 4111
[7] Johnston H C and Hallet N C 1953 *J. Am. Chem. Soc.* **75** 1467
[8] Stephenson C C, Rice D W and Stockmayer W H 1953 *J. Chem. Phys.* **21** 1311
[9] Łodziana Z and Vegge T 2004 *Phys. Rev. Lett.* **93** 145501
[10] Vajeeston P, Ravindran P, Kjekshus A and Fjellvåg H 2005 *J. Alloys Compds.* **387** 97
[11] Shevlin S A, Cazorla C and Guo Z X 2012 *J. Chem. Phys.* C **116** 13488
[12] Vajeeston P, Ravindran P, Vidya R, Fjellvag H and Kjekshus A 2003 *Appl. Phys. Lett.* **82** 2257
[13] Babanova O A, Soloninin A V, Stepanov A P, Skripov A V and Filinchuk Y 2010 *J. Chem. Phys.* C **114** 3712
[14] Kang J K, Lee J Y, Muller R P and Goddard W A III 2002 *J. Chem. Phys.* **121** 21
[15] Soulié J-P, Renaudin G, Černý R and Yvon K 2002 I. Crystal structure *J. Alloys Compd.* **346** 200
[16] Züttel A, Rentsch S, Fischer P, Wenger P, Sudan P, Mauron P and Emmenegger C 2003 *J. Alloys Compd.* **356** 515
[17] Filinchuk Y and Chernyshov D 2007 *Acta. Cryst.* A **63** 240
[18] Filinchuk Y, Chernyshov D and Černý R 2008 *J. Phys. Chem.* C. **112** 10579
[19] Filinchuk Y, Chernyshov D, Nevidomskyy A and Dmitriev V 2008 *Angew, Chem. Int. Ed.* **47** 529
[20] Miwa K, Ohba N, Towata S-I, Nakamori Y and Orimo S-I 2004 *Phys. Rev.* B **69** 245120
[21] Frankcombe T J, Kroes G-J and Züttel A 2005 *Chem. Phys. Lett.* **405** 73
[22] Kumar R and Cornelius A 2005 *Appl. Phys. Lett.* **87** 261916
[23] Filinchuk Y, Talyzin A V, Chernys hov D and Dmitriev V 2007 *Phys. Rev.* **B76** 092104
[24] Kim E *et al* 2007 *J. Phys. Chem.* B **111** 13873
[25] Caputo R, Tekin A and Sol. J 2011 *Stat. Chem* **184** 1622
[26] Lee G, Lee J-Y and Kim J S 2006 *Sol. Stat. Com.* **139** 516
[27] George L, Drozd V, Couvy H, Chen J and Saxena S-K 2009 *J. Chem. Phys.* **131** 074505
[28] Belskii V K, Bulychev B M and Golubeva A V 1982 *Acta Crystallogr. Sect. B: Struct. Crystallogr. Cryst. Chem.* **38** 1254
[29] Arroyo y de Dompablo M E and Ceder G 2004 *J. Alloys Compds.* **364** 6

[30] van Setten M J, Popa V A, de Wijs G A and Brocks G 2007 *Phys. Rev.* **B75** 035204
[31] Arroyo y de Dompablo M E and Ceder G 2005 *Z. Anorg. Allg, Chem.* **631** 1982
[32] Peles A, Alford J A, Ma Z, Yang L and Chou M Y 2004 *Phys. Rev.* B **70** 165105
[33] George L and Saxena S K 1996 *Int. J. Hydrogen Energy* **11** 5454
[34] Blaha P, Schwarz K, Madsen G K H, Kvasnicka D and Luitz J 2001 *WIEN2K, Karlheinz Schwarz* (Wien, Austria: Techn. Universitat) ISBN 3-9501031-1-1-2
[35] Perdew J P, Burke S and Ernzerhof M 1996 *Phys. Rev. Lett.* **77** 3865
[36] Engel E and Vosko S H 1993 *Phys. Rev.* B **47** 13164
[37] Jepsen O and Andersen O K 1971 *Sol. Stat., Commun.* **9** 1763
[38] Wilson J A and Yoffe A D 1969 *Adv., Phys.* **18** 193
[39] Born M and Huang K 1954 *Appendix IV* (Oxford: Clarendon Press) 391
[40] Khan M A, Kashyap A, Solanki A K, Nautiyal T and Auluck S 1993 *Phys. Rev.* B **23** 16974
[41] Tributsch H 1977 *Z. Naturforsch.* A **32** 972
[42] Wooten F 1972 *Optical Properties of Solids* (New York: Academic press) ch 5
[43] Fischer P and Zuttel A 2004 *Mater. Sci. Forum* **443–444** 287
[44] Hauback B C, Brinks H W and Fjellvåg H 2002 *J. Alloy. Compd.* **346** 184–9
[45] Murnaghan F D 1944 *Proc. Nat. Acad. Sci. USA* **30** 244
[46] Filinchuk Y and Hagemann H 2008 *Eur. J. Inorg. Chem.* 3127
[47] Kumar R S and Cornelius A L 2005 *Appl. Phys. Lett.* **87** 261916
[48] Sundqvist B and Andersson O 2006 *Phys. Rev.* B. **73** 092102
[49] Davis R L and Kennard C H L 1985 *J. Sol. Stat. Chem.* **59** 393
[50] Filinchuk Y, Chernyshov D and Dmitriev V 2008b *Z. Kristallogr.* **223** 649
[51] Sundqvist B 2009 *Sol. Stat. Phenomena* **150** 175
[52] Talyzin A V and Sundqvist B 2004 *Phys. Rev.* B **70** 180101
[53] Chellappa R S, Chandra D, Gramsch S A, Hemley R J, Lin J F and Song Y 2006 *J. Phys. Chem.* B **110** 11088
[54] Reshak A H, Charifi Z and Baaziz H 2008 *Eur. Phys. J.* B **60** 463
[55] Charifi Z, Baaziz H, El Haj Hassan F and Bouarissa N 2005 *J. Phys: Condensed Matter* **17** 4083
[56] Orgaz E, Membrillo A, Castaneda R and Aburto A 2005 *J. Alloys Compd.* **404** 176
[57] Graetz J 2012 *ISRN Materials Science* **2012** 1 ID 863025
[58] Shan W, Walukiewicz W, Ager J W III, Haller E E, Geisz J F, Friedman D J, Olson J M and Kurtz S R 1999 *Phys. Rev. Lett.* **82** 1221
[59] Penn D R 1962 *Phys. Rev.* B **128** 2093–7